Application of ANN and RSM techniques in optimal parameter evaluation for turbidity removal from abattoir effluent using valorized chicken bone coagulant

Abstract

Chicken bone coagulant (CBC) containing high grade hydroxyapatite (HPA) has been applied in the coag-flocculation of abattoir effluent. The influence of process variables (pH, initial concentration, dosage, Temperature, and settling time) on the effluent final turbidity was investigated. Also, the accuracies of two modelling techniques (Response surface methodology, RSM and Artificial neutral network, ANN) in predicting the non-linear nature of the system were compared. The optimization result indicates a final turbidity of 4.96 mg/L (corresponding to 98.28 % removal efficiency) at pH = 6.7, dosage = 1.003 g/L, initial conc. = 182.2 mg/L, coagulation temp. = 345 K and settling time of 36 min. Meanwhile, effluent pH was spotted as the most significant variable, with p-value <0.01%. Furthermore, the error analysis result portrayed the supremacy of ANN over RSM in data prediction accuracy as it signified lower error values (Mean square error, MSE = 13.11 and Absolute average relative deviation, AARD = 1.43%) when compared to those of RSM (MSE = 37.78, AARD = 5.93%). Thus, it was demonstrated that ANN is a better tool for optimization study of the present system.

Keywords: Abattoir-effluent, Turbidity, Hydroxyapatite, Chicken Bone, Artificial Neural Network

1. Introduction

Fresh water is one of the most vital elements needed for human survival and sustenance of life in general. Even as population growth and rapid urbanization has resulted in an increased demand for existing fresh water. The contamination of the available fresh water sources remains the major challenge facing water resource users and also threatens the preservation of natural ecosystems. This challenge of ensuring the availability of fresh water for the teeming human population is further heightened by the discharge of harmful contaminants into the already stressed fresh water bodies, thereby polluting them.

The activities of abattoir industry provide a means to the major source of protein supply for Nigeria's large population and also remain a major source environmental pollution. The industry contributes about 6 % of the country's total gross domestic product (GDP) and about 20 % of the agricultural GDP (Mshelbwala, 2013; Ogbeide, 2015: Ohale et al., 2022a). The basic meat production processes occurring in an abattoir includes; slaughtering of animals, washing, butchering and subsequent packaging of the raw meat for further processing or consumption.

These processes generate large volume of contaminated water often referred to as abattoir-effluent. The abattoir-effluent is often characterized by varieties of organic pollutants originating from the paunch, feces, fat and lard, grease, undigested food, blood, suspended material, urine, soluble proteins, manure, grit, condemned meat and colloidal particles. These pollutants are responsible for the characteristics dark colour and offensive odour of abattoir-effluent, as well as their poor bacteriological standards (Obi et al., 2022; Ohale et al., 2022a). The discharge of abattoir-effluent into the environment without adequate treatment contribute greatly to the degradation of the aquifer and pollution of streams and irrigation water with high organic matter (Obi et al., 2022).

Several researchers have successfully used various approaches for the treatment of abattoir-effluent at laboratory and pilot scale experiments. Sequencing batch reactors, anaerobic treatment process, electro-coagulation, aerated lagoon system, high rate algal ponds, treatment with halophytes, and integrated biological treatment system are among the studied treatment processes (Kundu *et al.,* 2013; Bazrafshan *et al.,* 2022; Obi et al., 2022; Ohale et al., 2022a). Among these processes, anaerobic treatment process has been widely adopted for the treatment of abattoir-effluent. However, the efficiency of anaerobic treatment processes is limited due to the high energy required for aeration, production of excess sludge, time-consuming treatment rate resulting from accumulation of suspended solids, and floating fats in the reactor (Menkiti *et al.,* 2015). Owing to the limitations of anaerobic treatment process, coagulation and flocculation remains a choice method for many researchers in the management of highly turbid effluents (Menkiti *et al.,* 2015; Ohale et al., 2020). This could be due to their cost effectiveness and flexibility of operation. The purpose of coagulation and flocculation process is to form large floccus that are denser than the carrier effluent so they can settle and be separated by decantation. The entire coagulation process comprises of three separate and sequential steps; coagulant formation, particle destabilization, and inter-particle collisions (Menkiti et al., 2016; Ohale et al., 2020; Obi et al., 2022). The major coagulation process parameters are coagulant dosage, coagulation temperature, effluent pH and initial effluent concentration. Studies by Al-Mutairi, *et al.,* (2004) and Amuda & Alade, (2006), investigated the use of aluminium salt and poly-aluminium chloride, respectively as active coagulants for the remediation of abattoir effluent. Aquilar, *et al.,* (2005), reported a maximum turbidity removal efficiency of 87 % by using alum without coagulant aids in the treatment of abattoir effluent. Furthermore, Amudaa & Alade, (2006) achieved a substantial reduction in COD from abattoir effluent using 1000 mg/L of alum. Mahtaba, *et al.,* (2009) reported 99 % removal of suspended solids by using 400

mg/L of alum and 30 mg/L of polymer. However, the negative health implications of the use of these chemical coagulants have been pointed out. According to Katayon, *et al.,* (2006), Alzheimer's disease, surplus sludge production, cost ineffectiveness and introduction of considerable changes in the chemical properties of water due to reactions with the OH^- and alkalinity of water are some of the adverse implications associated with the use of chemical coagulants. Hence, the frequent problems relating to the use of metal salts and chemical coagulants could be significantly mitigated via the use of natural coagulants (Katayon, *et al.,* 2006).

A variety of natural coagulants have been developed by many researchers for the remediation of highly turbid waste water. Some of which are crab-shell chitin (Saritha, et al., 2015), snail shell extract (Menkiti &Ejimofor, 2016), Dromedary bone (Ghedjemis et al., 2022), Periwinkle shell (Menkiti, *et al.,* 2016). Recently, the use of animal bone for the treatment of various of types of wastewater has gained the attention of researchers (Choumane et al., 2017; Brazdis et al., 2021). Studies have shown that animal bones contain an active ingredient called hydroxyapatite (HAP), which has been proven to be very useful in surface driven wastewater treatment processes such as coagulation (Ghedjemis et al., 2022; Brazdis et al., 2021). Hydroxyapatite (HAP) has a highly stable calcium phosphate hexagonal structure which can withstand extreme conditions of temperature and pH. Many researchers have successfully used HAP in removal of heavy metals (Marrane et a., 2022; Brazdis et al., 2021), turbidity (Choumane et a., 2017), and dye wastewater (Ghedjemis et al., 2022). Therefore, in a bid to further proffer solution to the environmental pollution associated with the possible indiscriminate discharge of abattoir effluents; this current study is imperative. The study investigates the synthesis and potential utilization of chicken bone (CB) coagulant in the coag-flocculation treatment of abattoir-effluent. Although the effectiveness of numerous natural coagulants in the treatment of abattoir effluent via coag-flocculation process have been widely reported in literature, however, to the best of our knowledge, there has not been any reported use of chicken bone coagulant (CBC) in the treatment of abattoir-effluent.

In the past, "one-factor at a time" (OFAT) was the commonest approach adopted by many researchers in the search for optimal experimental conditions. However, the OFAT approach is usually cumbersome and time consuming. Also, it rarely satisfies the search for a desired optimum. These drawbacks associated with the use of OFAT approach can be avoided by using empirical design methods of analysis. Recently, RSM and ANN as an empirical design optimization tool have been jointly adopted in effluent treatment studies (Onu et al., 2022a; Ohale et al., 2017; Nwadike et al., 2020; Onu et al., 2022b). RSM is applied in industrial

processes for the purpose of either producing high quality products or operating a process in a more economical manner (Onu et al., 2021). The main objective of RSM is to optimize an unknown and noisy function through simpler approximation functions which are sustainable over a confined region using experimental designs. Several researchers have reported the successful application of RSM technique in the optimization of process conditions (Onu et al., 2020; Emembolu et al., 2022). Furthermore, due to the multidisciplinary advancement of modern analytical techniques, artificial neural networks (ANNs) as typical artificial intelligence (AI) algorithms have become an envisaged approach for modeling robust and non-linear systems (Ohale et al., 2022a). The most important feature of ANN is its generic structure and ability to learn from historical data. It is often believed that ANN could require much more number of experiments than RSM to build an efficient model. However, studies have shown that a relatively less volume of data could still be used if the data are statistically well distributed in the input domain (Shafi et al., 2018). Also, the experimental data of any well-defined RSM would be sufficient to build an effective ANN model. Literature studies have shown that ANN model consistently worked better than RSM model in predicting the response of non-linear systems (Pakravan et *al.,* 2015; Sodeifian et *al.,* 2016). The study therefore intends to critically analyze and derive a model for final turbidity reduction of abattoir-effluent using the most significant factors. The accuracy of ANN and RSM techniques in modelling the coag-flocculation process will be comparatively assessed. Also, the formulated objective function would be optimized using hybrid ANN-Genetic algorithm (ANN-GA) technique.

2 Materials and Methods

2.1. Materials

The abattoir effluent was collected from a local slaughterhouse located at Amasea in Anambra state, Nigeria. Chicken bones were collected from refuse were collected from fast food waste around Awka, in Anambra state, Nigeria. Furthermore, analytical grade chemical reagents utilized in the experiment were obtained from the Chemical Engineering Laboratory of Nnamdi Azikiwe University, Awka, Nigeria.

2.2. Sample pre-treatment and storage

The collected abattoir-effluent was preserved by refrigeration. Prior to each stage of treatment, the effluent was allowed to sediment for 24 h and afterwards decanted. Sediments which are majorly composed of very fine particles which could not undergo gravity settling were afterwards stored (in refrigerator) for coag-flocculation treatment. The chicken bones (CB) were washed with deionized water to remove the marrow and inherent dirt, afterwards they

were cut into fragments of 2–5 g mass, boiled in distilled water and dried at a temperature of 90 ^{0}C for 8 h onto constant weight.

2.3. Extraction of active coagulant

The procedure reported by Brezinska-Miecznik et al., (2015) was adopted in the extraction of hydroxyapatite (HPA) from chicken bones (CB). Briefly, the dried CB fragments were treated with 4M NaOH solution at 90 ^{o}C for 12 days. The sample to solution ratio of the treatment was kept 1 g of sample to 90 cm^3 of solution. At the end of the treatment procedure, the treated samples were repeatedly washed with distilled water until the pH of the filtrate approached neutrality. The washed samples were dried at 150 ^{o}C for 10 h, after which they were crushed using mechanized crusher to particle size of 70 μm (using a Particle Size Distribution Analyzer - Model 117.08, MALVERN Instruments, USA) and then stored in an air tight container.

2.4. Abattoir-effluent sample calibration and characterization

In order to establish a logical link between the units of turbidity (NTU) and those of concentration (mg/L), serial dilution of the raw effluent was obtained. For each of the dilute solutions, characteristic concentration in NTU and the corresponding amount (mg) per volume of the sample were obtained using turbidity meter (Hanna Instruments, Model: LP2000) and sensitive weighing balance (JA-SARIES, Model: JA203H), respectively. Results obtained from the effluent calibration were supplied in section 3.1. Furthermore, American Public Health Association (APHA) standard procedure as reported by Clesceri, *et al.*, (1998) was adopted for the physicochemical characterization of the abattoir-effluent. Elaborate discussion of findings from the physicochemical characterization of the effluent was presented in section 3.2.

2.5. Coagulant characterization

The physicochemical properties and degree of effectiveness of the chicken bone coagulant (CBC) extraction process was ascertained by characterization. The structural vibration, topographical stabilization, and the crystallinity of the CB and CBC were determined using Fourier Transform Infra-red Spectroscopy (FTIR) (ThermoNicolet Nexus Model 470/670/870), Scanning Electron Microscopy (SEM) (Model Zeiss Evo®MA 17 EDX/WDS microscope), and X-ray Diffraction (XRD) (PHILIPS X PERT X – RAY diffraction unit with Cu Kr radiation), respectively. All the instrumental analysis was carried out according to ASTM E1508 and ASTM E168 standards.

2.6. Jar test procedure and experimental design

The jar test procedure was carried out based on standard Bench scale nephelometric technique for investigation of water and waste water (AWWA, 2005 and WST, 2003), using Model LP-2000 Hanna Instruments Turbidimeter, Search tech Instruments 78 HW-1 magnetic stirrer and PHS-3C 005399 pH meter.

The pH of the effluent was adjusted to pH 3, 4, 6, 8 and 10 using 1 M H_2SO_4 and 1 M NaOH, after which appropriate amounts (0.7, 1.0, 1.6, 2.2, and 2.5 g/L) of CBC were added to each 500 ml beaker containing different concentrations of abattoir effluent (100, 184, 350, 517, 600 mg/L) as illustrated in Table 2.

Central Composite Design (CCD) was applied in this work to model the coagulation process of turbidity removal from abattoir effluent. The design consists of a 2n factorial or fraction (coded to the usual ±1 notation) augmented by 2n axial points (±α, 0, 0,..., 0), (0, ±α, 0,..., 0),..., (0, 0,..., ±α), and n_c centre points (0, 0, 0,..., 0). The statistical relevance of each parameter was evaluated using analysis of variance (ANOVA) (Ohale, *et al.*, 2017). If all variables are assumed to be measurable, the response surface can be expressed as Eq. (1). RSM optimizes the response variable (y) and searches for a suitable approximation of the functional relationship between the independent variables and the response surface.

$$y = b_0 + \sum b_i X_i + \sum b_{ii} X_{ii}^2 + \sum b_{ij} X_i X_j + \varepsilon \quad (1)$$

For statistical analysis, the experimental variable X_i has been coded as x_i as shown in Eq. 2:

$$x_i = \frac{X_i - X_n}{\Delta X_i} \quad (2)$$

Where x_i is the coded value (dimensionless) of the *ith* independent variable, X_i is the un-coded value of the *ith* independent variable, X_n is the real value of an independent variable at the centre point and ΔX_i is the step change value of the real variable *i*. The relationship between the coded value and level of variance is presented in Table 1.

Table 1: Relationship between coded value and the level of variance

Coded value	Level of variance
-α	X_{min}
-1	$[(X_{min} + X_{max})/2] - [(X_{max} - X_{min}) / 2b]$
0	$[(X_{min} + X_{max})/2]$
+1	$[(X_{min} + X_{max})/2] + [(X_{max} - X_{min}) / 2b]$
+ α	X_{max}

Where; X_{min} and X_{max} are minimum and maximum values of X, respectively. Applying the relationships in Table 1, the values of the codes were calculated and shown in Table 2.

Table 2: Levels of independent variables for CCD experimental design

Independent variables		Symbol	Coded variable levels				
			-α	**-1**	**0**	**+1**	**+α**
pH		x_1	3	4	6	8	9
Dosage	g/L	x_2	0.7	1.0	1.6	2.2	2.5
Initial conc.	mg/L	x_3	100	184	350	517	600
Temperature	K	x_4	301	310	327.5	345	354
Settling time	min	x_5	6.3	15	32	50	59

The experimental plan was generated using the Design-Expert program 11.0 trial version (Stat-Ease Inc., Minneapolis, USA).

2.7 Artificial neural network (ANN)

Multi Layer Perceptron (MLP) with Marquardt Levenberg algorithm using back propagation was used in the development of ANN. The MLP was executed in MATLAB (The mathworks, inc., 2009 b), with five input variables making up the input layer and the final turbidity representing the only output neuron. Neuron input is comprised of its bias and the sum of its weighted input. The mathematical expression describing the neuron is given as Eq. (3);

$$Y_i = \sum_{i=1}^{n} x_i \omega_i + \theta_i \qquad (3)$$

Where; Y_i is the net input to the node, i in the hidden layer, $w_i (i = 1, n)$ are the connection weights, θ_i is the bias and x_i is the input parameter. The weighted output was subjected to a nonlinear activation function, the logistic output function as shown in Eq. (4);

$$f(sum) = \frac{1}{1 + \exp(-sum)} \qquad (4)$$

The architecture of the artificial neural network used in this work as presented in Fig. 1 shows that the output from the input layer formed an input for the hidden layer. Similarly, the output layer receives an input from the hidden layer.

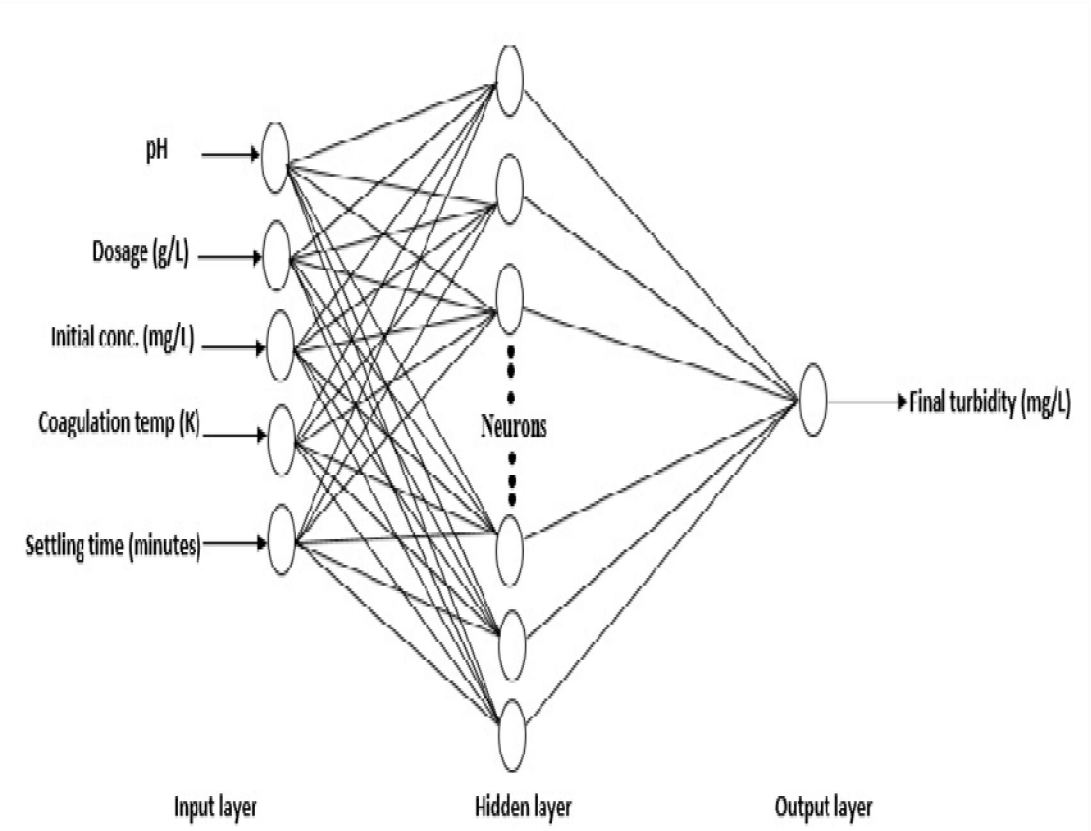

Fig. 1: Architecture of the developed artificial neural network

The hidden number of neurons was arbitrarily varied from 2 to 12, and a suitable number was chosen via regression and error function tests (see Eqs. 5 & 6, respectively) on the outputs obtained (by varying the number of neurons). The tests compare the deviation of their predictions from the experimental values (Ohale et al., 2022b).

$$R^2 = 1 - \frac{\sum_{i=1}^{i=n}\left(y_{i,predic} - y_{i,\exp}\right)^2}{\sum_{i=1}^{i=n}\left(y_{i,\exp} - y_{av}\right)^2} \tag{5}$$

$$RMSE = \sqrt{\frac{\sum_{i=n}^{n}\left(y_{i,predic} - y_{i,\exp}\right)^2}{n}} \tag{6}$$

Where n is the number of data points, $y_{i,predic}$ is the network prediction at a specific number of hidden neurons, $y_{i,\exp}$ is the real experimental response, y_{av} is mean value of experimental data and *i* is the data index.

3. Result and discussions

3.1 Calibration of Abattoir effluent

The result of effluent calibration was presented in Fig. 2. Visual inspection of the plot line showed the existence of a directly proportional relationship between the amount of particles (mg) and the turbidity (NTU). Linear correlation models given in Eqs. (7) and (8) were obtained from the calibration analysis and were subsequently employed in converting the concentration of abattoir effluent from NTU to mg/L.

$$C_{mg/L} = 1.841 C_{NTU} - 11.368 \quad (7)$$

$$C_{mg/L} = 1.81 C_{NTU} \quad (8)$$

Where; $C_{mg/L}$ and C_{NTU} are the effluent concentrations in mg/L and NTU, respectively. Eq. 8 strictly applies to abattoir effluent with very low concentrations (NTU < 6.18).

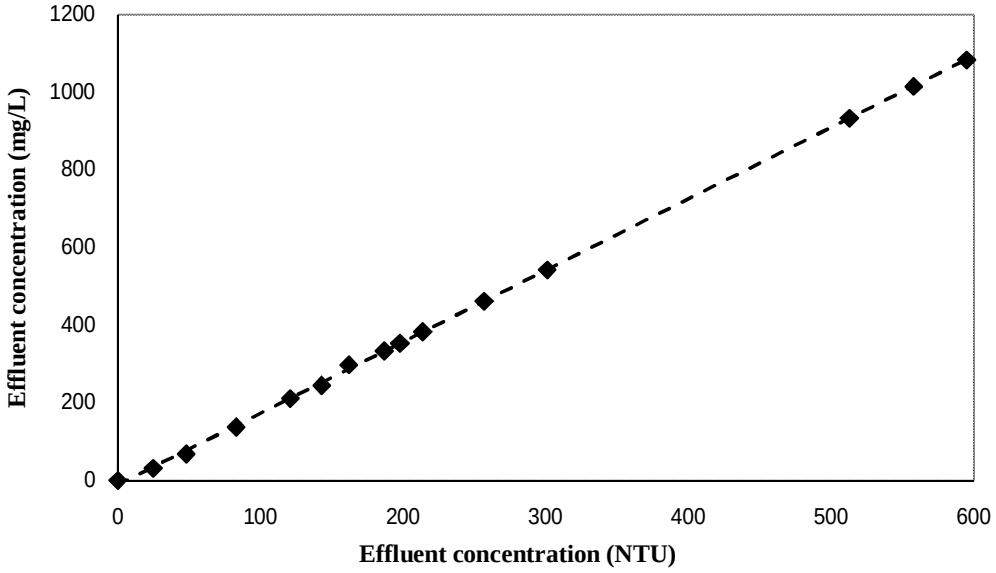

Fig. 2: Abattoir-effluent calibration plot

3.2. Waste water characteristics

The physicochemical characteristics of the raw effluent prior to treatment were presented in Table 3. A close observation of Table 3 shows that only the effluent pH is within the permissible discharge limit as stipulated by the Environmental Protection Act (EPA). The total suspended solids (TSS) and the total solids (TS) which bear major influence on the effluent turbidity, were significantly higher than the tolerable EPA threshold for effluent discharge; thus justifying the need for treatment.

Table 3: Physicochemical characteristics of abattoir-effluent

Parameters	Concentration	FEPA
Initial turbidity concentration (mg/L)	599	<100
Total suspended solids (mg/L)	1030.8	<100
Total solids (mg/L)	1614.8	<500
Biological oxygen demand $(mg/L)_5$	220	210
Chemical oxygen demand (mg/L)	692	<180
pH	7.5	6 – 9
Odour	Objectionable	Odorless
Colour	Dark red	-

3.3 Instrumental characterization of the CSC

3.3.1 FTIR spectra analyses

The FTIR spectra of the CB and CBC are shown in Figs. 3a and 3b, respectively. Visual inspection of the spectra results shows that the obtained CBC spectra fall within the frequency of 3325 – 650 cm^{-1}. According to Coutts, 2008, the observation peaks below 600 cm^{-1} are not applicable for characterizing wavebands. The vibrational peak at 663.5 cm^{-1} which is attributed to OH functional group, became more conspicuous in CBC following NaOH treatment. The absorption band intensity at 1241.2 cm^{-1} in the raw CB, shifted to 1244.9 cm^{-1} after the HAP extraction process. This waveband (1241.2 cm^{-1}) demonstrates the presence of CO_3^{2-} which indicates a major characteristic property of HAP. The peak at 1032.5 cm^{-1} indicates the presence of C – O bending of the glucose molecule due to C – O – C linkage. The presence of phosphorus compound (P – F stretching) is displayed on 898.3 cm^{-1}, while its presence on the

CBC (HPA) spectra shows the presence of N – H wagging band of the protein compounds. The C–O stretching band at 1159.2 cm^{-1} indicates the presence of anhydrides in the CBC; while those at 3324.8 cm^{-1} suggest the presence of N – H amides (Brzezińska-Miecznik et al., 2014).

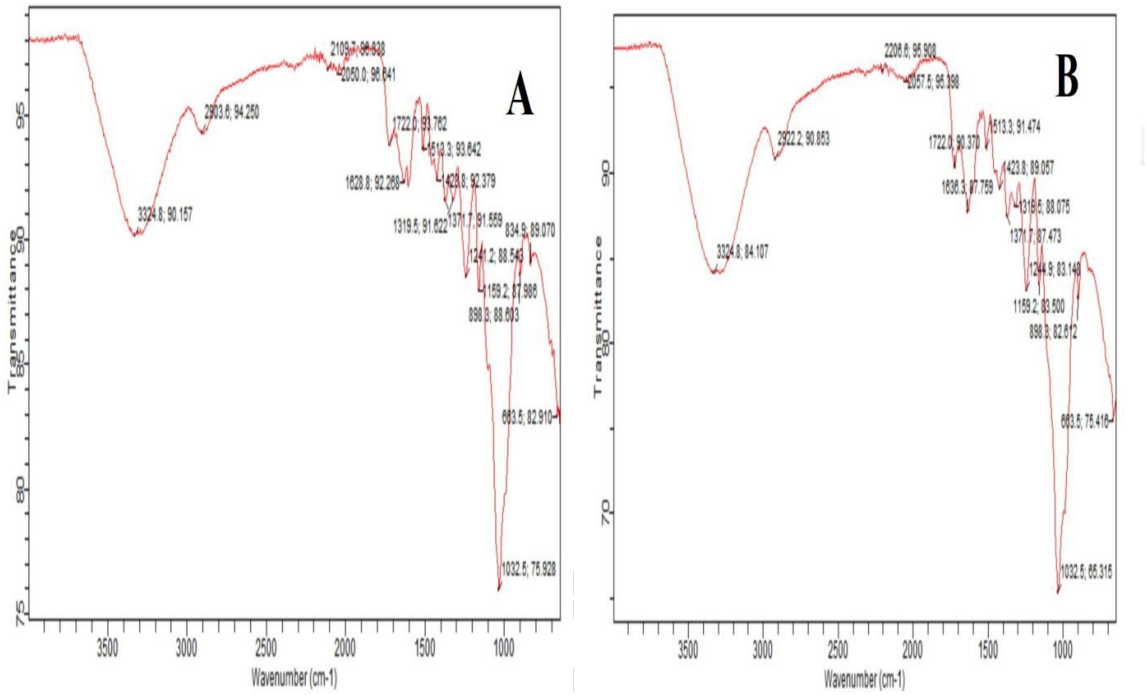

Fig. 3: FTIR spectra of (a) CB (b) CBC

3.3.2 SEM image analyses

Figs. 4 (a & b) represents the scanning electron micrograph of CB and CBC, respectively. The SEM image of the CB reveals the appearance of irregular platelet. This suggests that the CB possesses rough edges, with crispy properties; a unique feature of animal tissues with high calcium content. Similarly, the comparison of Fig 4b and Fig 4a shows characteristic improvement in the morphological features. Some of these improvements such as the formation of better cohesion, reduced individual lamella and the presence of a highly porous dark field matrix could be a direct consequence of HPA extraction process. The improved porous property is important for enhanced particle sticking required for surface phenomenon driven matrices like coagulation.

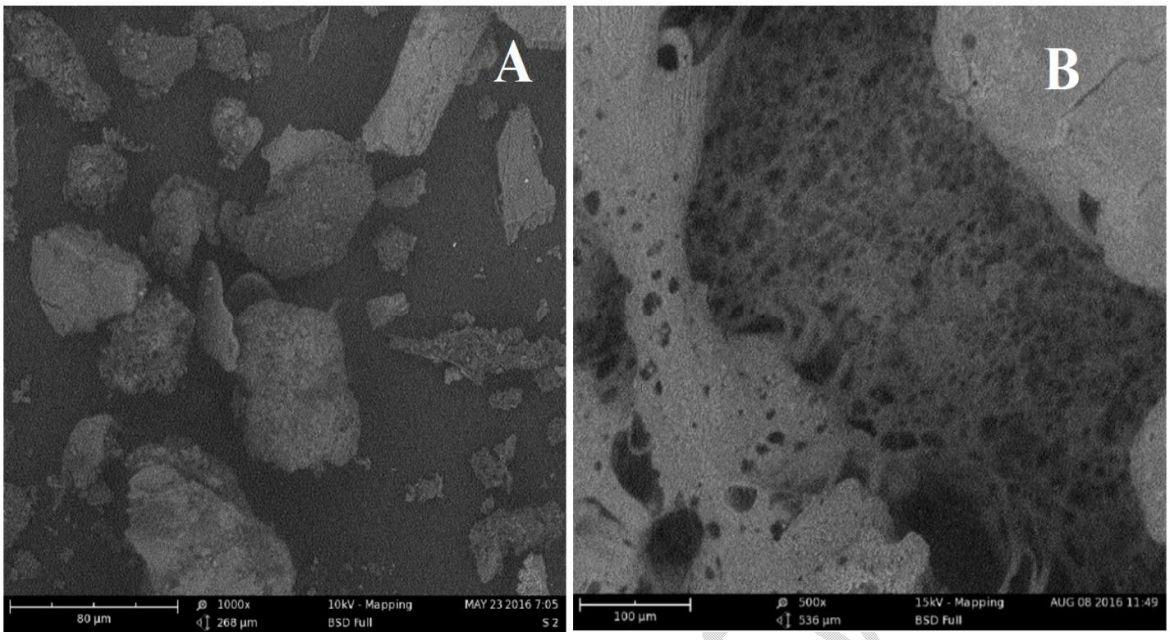

Fig. 4: SEM micrograph of (a) CB (b) CBC

3.3.3. XRD analyses

The polymorphic features of a compound with different crystalline structures are determined using x-ray diffraction technique. The XRD pattern of CB and CBC are depicted in Figs. 5 (a & b), respectively. The XRD pattern of CB depicts a well organized spectral pattern with strong reflections 2Θ values of around 8 – 10, 17 – 19, 23 – 35 and 33 – 37^0. While the XRD pattern of CBC shows similar reflections as those of CB at 2Θ values but with low intensity peaks. The unorganized nature of the CBC spectral pattern and its low intensity values indicates that the CBC is a less crystalline poly-morph when compared to CB.

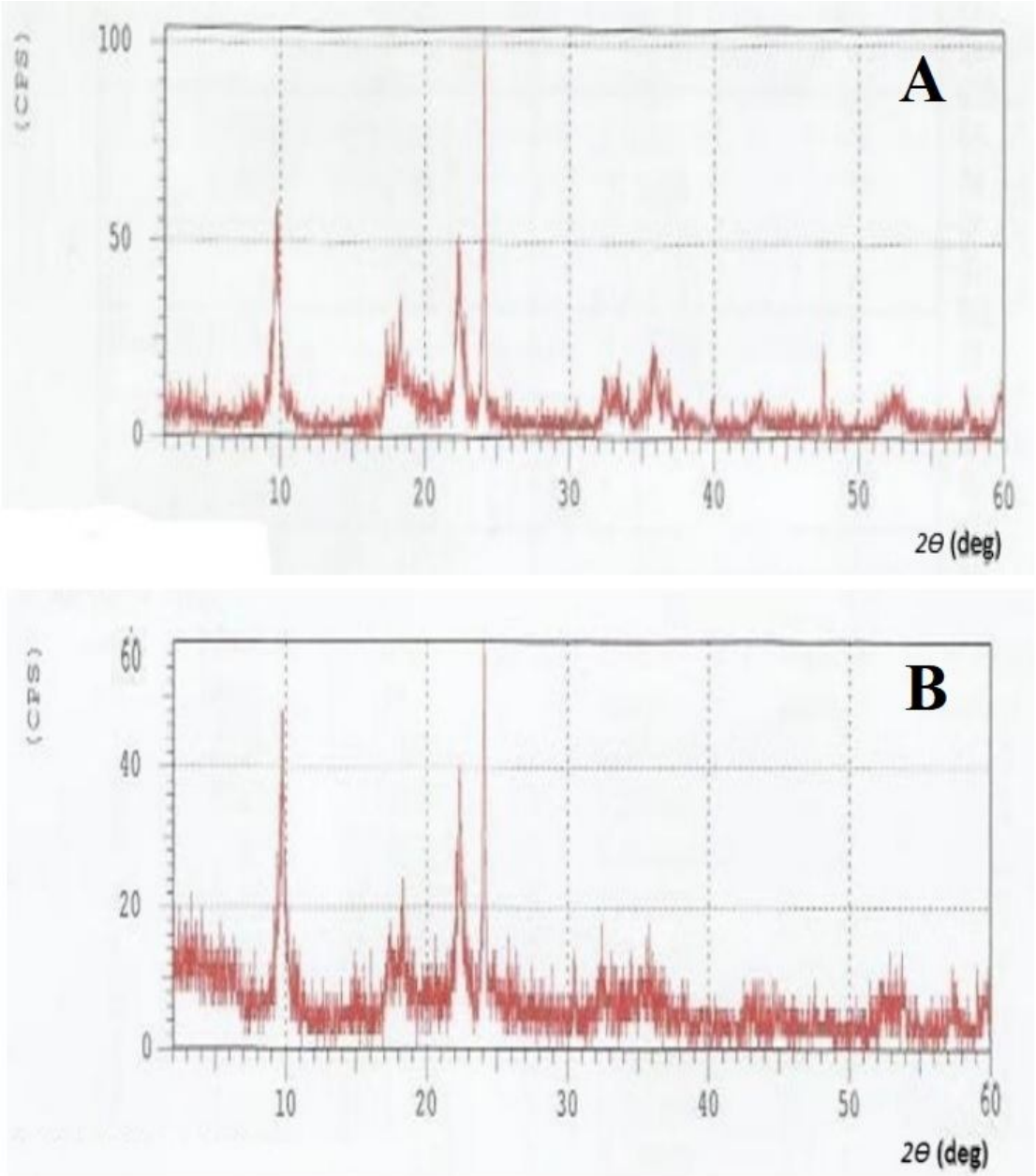

Fig. 5: XRD pattern for (a) CB (b) CBC

3.4. RSM modelling

The combined effects of effluent pH, coagulant dosage, initial concentration, coagulation temperature and settling time on effluent turbidity reduction was studied using central composite design. The five-input experimental design produced 32 runs (consisting of 16 factorial points, 10 axial and 6 centre points); as well as the predicted values of percentage turbidity removal are presented in **Table 4**. Also, **Table 5** shows the relevant parameters generated from the analysis of variance (ANOVA). It should be noted that ANOVA technique

employs the p-value and F-value to determine the adequacy and fitness of the empirical model. Hence, by comparing the model and lack of fit parameters, an f-value of 189.043 and a low p-value of 0.0001 as shown in **Table 5** implies that the model is significant. The model p-value of 0.0001 indicates that there is only 0.01% chance that the model f-value could occur due to noise. The values of "prob > f" less than 0.0500 indicate that model terms are significant. Thus, $x_1, x_2, x_3, x_5, x_1x_3, x_1x_4, x_1x_5, x_2x_4, x_2x_5, x_3x_4, x_3x_5, x_1^2, x_2^2 and x_5^2$ are significant model terms. The lack of fit f-value of 0.91 implies the lack of fit is not significant relative to pure error, there is 58.59% chance that a lack of fit f-value this large could occur due to noise. This value of lack of fit implies that the model is well fitted (Ohale et al., 2022a). The smaller the magnitude of p-value, the greater the significance of the corresponding model term. From **Table 5**, effluent pH and coagulation temperature have the highest and the least influence respectively, on the final turbidity of the effluent, which is in agreement with the findings of other researchers (Menkiti et al., 2015, Ohale et al., 2020). The predicted R-squared of 0.9675 is in reasonable agreement with the adjusted R-squared of 0.9765 because they are < 0.2 apart from each other (Ohale et al., 2022a).

Table 4: The CCD matrix along with the experimental and predicted values

Std order	Point type	pH	Dosage (g)	Initial Conc. (mg/L)	Temp. (K)	time (min)	EXP	RSM	ANN
1	Factorial	-1	-1	-1	-1	1	197.9	201.1	197.9
2	Factorial	1	-1	-1	-1	-1	19.3	23.6	19.3
3	Factorial	-1	1	-1	-1	-1	167.9	171.1	167.9
4	Factorial	1	1	-1	-1	1	64.1	66.4	63.3
5	Factorial	-1	-1	1	-1	-1	294.7	300.7	294.7
6	Factorial	1	-1	1	-1	1	88.8	84.0	88.8
7	Factorial	-1	1	1	-1	1	117.1	113.2	118.7
8	Factorial	1	1	1	-1	-1	101.1	108.4	101.1
9	Factorial	-1	-1	-1	1	-1	30.8	32.3	30.8
10	Factorial	1	-1	-1	1	1	82.3	81.8	81.9
11	Factorial	-1	1	-1	1	1	137.0	135.3	137.0
12	Factorial	1	1	-1	1	-1	111.5	112.2	111.5
13	Factorial	-1	-1	1	1	1	156.6	157.8	156.6
14	Factorial	1	-1	1	1	-1	61.0	54.5	61.0
15	Factorial	-1	1	1	1	-1	424.1	418.5	424.1
16	Factorial	1	1	1	1	1	100.9	103.3	101.7
17	Axial	-1.5	0	0	0	0	285.3	283.6	285.3
18	Axial	1.5	0	0	0	0	118.1	115.7	118.1

19	Axial	0	-1.5	0	0	0	122.0	120.2	122.0
20	Axial	0	1.5	0	0	0	177.2	175.0	177.2
21	Axial	0	0	-1.5	0	0	47.8	48.9	47.8
22	Axial	0	0	1.5	0	0	144.0	155.5	144.0
23	Axial	0	0	0	-1.5	0	118.6	100.2	118.6
24	Axial	0	0	0	1.5	0	106.2	105.3	106.2
25	Axial	0	0	0	0	-1.5	66.5	60.3	66.5
26	Axial	0	0	0	0	1.5	5.9	8.1	5.9
27	Center	0	0	0	0	0	102.1	102.7	102.6
28	Center	0	0	0	0	0	95.8	102.7	102.6
29	Center	0	0	0	0	0	116.8	102.7	102.6
30	Center	0	0	0	0	0	93.1	102.7	102.6
31	Center	0	0	0	0	0	104.6	102.7	102.6
32	Center	0	0	0	0	0	94.1	102.7	102.6

Table 5: Analysis of variance table

Source	Sum of squares	dF	Mean square	F – value	p-value	
Model	214254.700	15	14283.647	189.043	< 0.0001	Significant
x_1	64261.909	1	64261.909	850.502	< 0.0001	
x_2	6852.238	1	6852.238	90.689	< 0.0001	
x_3	22364.783	1	22364.783	295.996	< 0.0001	
x_4	59.070	1	59.070	0.782	0.3897	
x_5	6205.656	1	6205.656	82.131	< 0.0001	
x_1x_3	9225.041	1	9225.041	122.093	< 0.0001	
x_1x_4	778.620	1	778.620	10.305	0.0055	
x_1x_5	7744.497	1	7744.497	102.498	< 0.0001	
x_2x_4	21981.617	1	21981.617	290.925	< 0.0001	
x_2x_5	15970.407	1	15970.407	211.367	< 0.0001	
x_3x_4	3257.661	1	3257.661	43.115	< 0.0001	
x_3x_5	20251.712	1	20251.712	268.030	< 0.0001	
x_1^2	22189.884	1	22189.884	293.682	< 0.0001	
x_2^2	4751.627	1	4751.627	62.887	< 0.0001	
x_5^2	11103.631	1	11103.631	146.956	< 0.0001	
Residual	1208.922	16	75.558			
Lack of Fit	806.794	11	73.345	0.912	0.5849	not significant
Std. Dev.	8.69		R-Squared	0.9944		
Mean	123.54		Adj R-Squared	0.9891		
C.V. %	7.04		Pred R-Squared	0.9765		

The final equation in terms of the coded factors is expressed as Eq. 9;

$$\begin{aligned} Final turbidity = {} & 102.73 - 55.99x_1 + 18.28x_2 + 35.88x_3 + 1.70x_4 - 17.40x_5 - 26.68x_1 \\ & + 6.9x_1x_4 + 22.0x_1x_5 + 37.07x_2x_4 - 31.59x_2x_5 + 15.85x_3x_4 - 39.53x_3x_5 \\ & + 43.08x_1^2 + 19.94x_2^2 - 30.48x_3^2 \end{aligned} \quad (9)$$

3.5. ANN modelling

Data set employed in ANN modeling was the same as those used in design of experiment (see Table 5). The graphical expression for the topological analysis is displayed in Fig. 6. Data partitioning as training set and test set were conducted to eliminate the issue of over-training and over parametrization. The 7 selected hidden neuron numbers produced the highest

correlation coefficient (0.988) and the least root mean square error (RMSE) value (0.3701). Also, the regression plot (Fig. 7) showed a relatively high correlation coefficient (R^2> 0.95); thus suggesting a good correlation between the experimental and ANN predicted values.

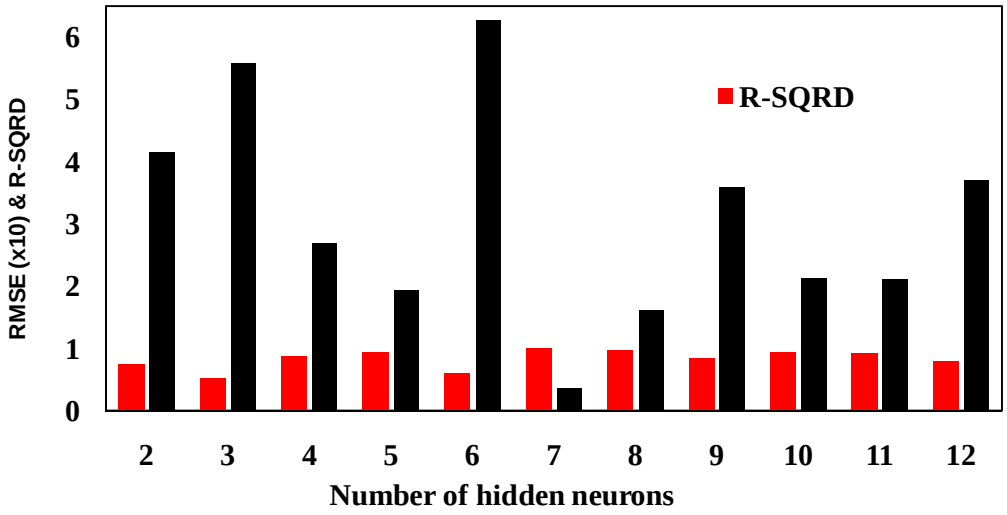

Fig.6: Effect of the neuron numbers in the hidden layer on the performance of the neural network

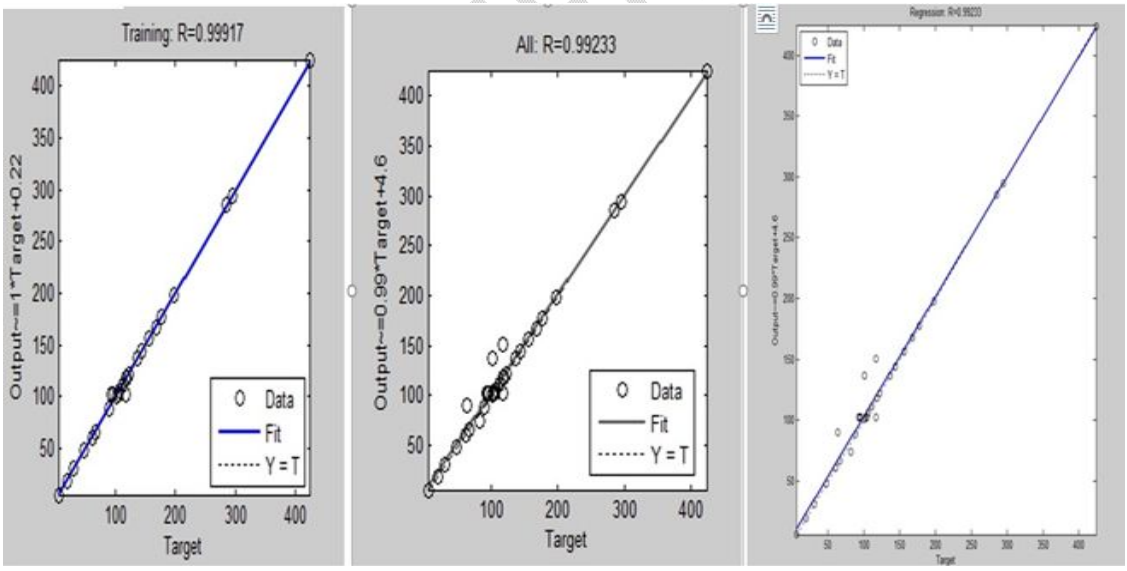

Fig. 7. Regression analysis for ANN predicted values versus exp. (target) values

3.6. Combined effect of operating parameters on final turbidity

The contour plot in Figs. 8 – 11 shows the result for the combined effects of various process variables on the abattoir effluent final turbidity. The reduced effluent final turbidity (80.3 mg/L)

observed in Fig. 8 was occasioned by an increased coagulant dose (from 1.0 g/L to 1.3 g/L) at a constant pH. Further increase in coagulant dosage (beyond 1.3 g/L) impacted the final effluent turbidity negatively, as the removal efficiency of suspended particles decreased significantly (see Fig. 11). The observed decrease in final turbidity with increase in the coagulant dose (up to 1.3 g/L) could be due to the availability of more active sites necessary for coagulation process. According to Menkiti and Ejimofor (2016), re-turbidization is caused by charge reversal due to over concentration of positively charged coagulant particles. This explains the reduction in turbidity removal efficiency (re-turbidization) when the coagulant dose is augmented beyond 1.3 g/L.

The combined effect of effluent pH and initial concentration is shown in Fig. 9. It could be observed that the coagulant displayed maximum turbidity reduction (58.6 mg/L) at neutral environment (pH 6.7) and at constant effluent initial concentration of 183.0 mg/L. Such observation could be explained by the fact that the buffer nature of the effluent tends to enhance the precipitation of the coagulant around neutral pH $(6.5 \leq pH \leq 7.0)$. However, the adjustment of the effluent pH either to the acidic or alkaline region was met with a significant reduction in turbidity removal efficiency$(final\ turbidity < 50.0\ mg/L)$. This is due to the disappearance of the effluent buffer nature at pH values outside the neutral environment; thus resulting in coagulant precipitation difficulties. The effect of initial effluent concentration shows that low initial concentration of raw effluent results in a low final turbidity. However, an increment in the effluent initial concentration results in low removal efficiency and a high final turbidity value. This phenomenon could be attributed to lack of sufficient active site for the removal of turbid particles at high concentration.

The effect of coagulation temperature and settling time is shown in the 2-D contour plot of Fig. 10. It could be observed that at high temperature, an accelerated settling rate was recorded; thus resulting in low final turbidity of the treated effluent. This observation could be explained by the fact that temperature increase bears positive effect on coagulation and flocculation process by altering the solubility and also reduces the effluent viscosity, thereby allowing for higher dispersion of CBC particles which aided floc formation and cell enmeshment (Ohale et al., 2020).

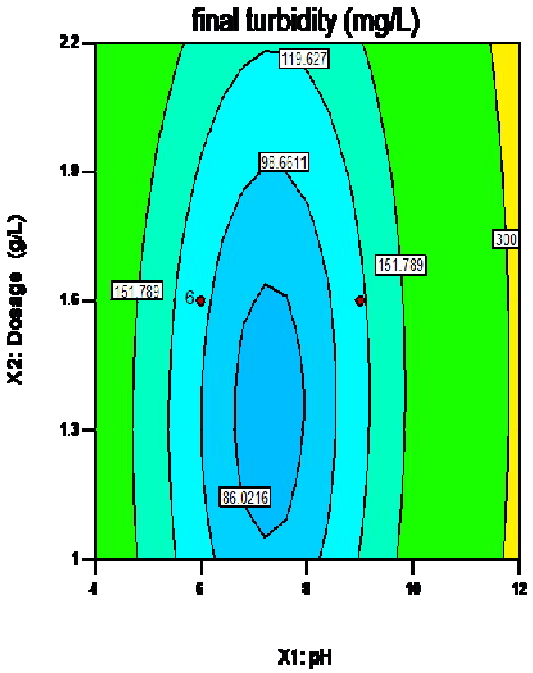

Fig. 8. 2D contour for the combined effects of coagulant dosage and effluent pH

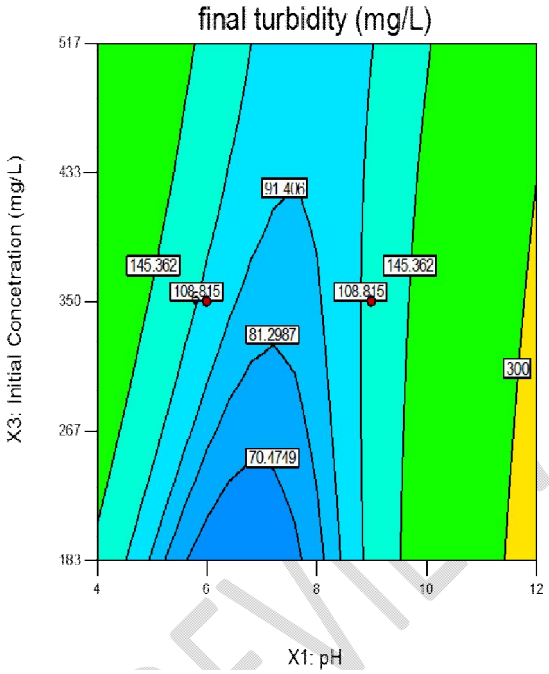

Fig. 9. 2D contour for the combined effects of effluent initial concentration and effluent pH

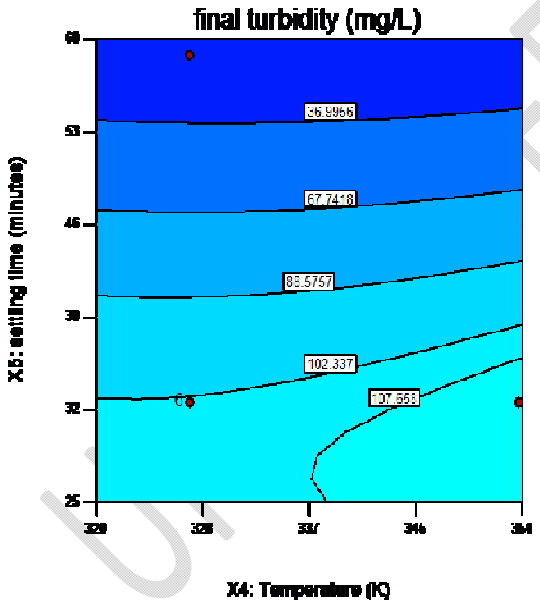

Fig. 10. 2D contour for the combined effects of settling time and coagulation temperature

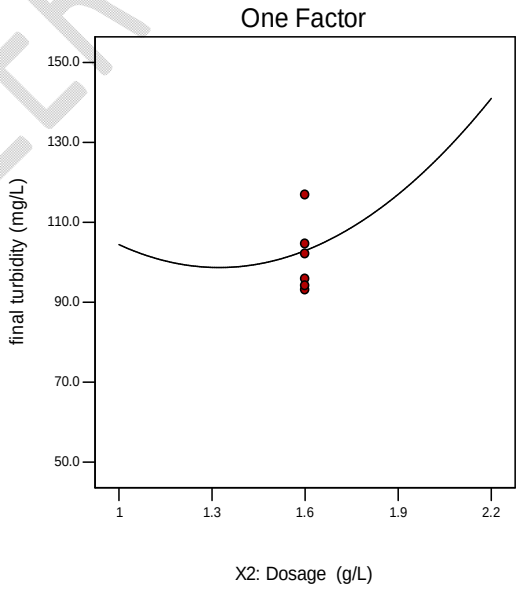

Fig. 11. Effect of coagulant dosage on the final turbidity.

3.7. ANN and RSM comparative analyses

In order to ascertain the superiority of either of the optimization tools (ANN and RSM) over the other in predicting the non-linear behavior of the present system, error functions were employed. The coefficient of determination (R^2), mean square error (MSE), and absolute average relative deviation (AARD) were the error functions used to compare the predictions accuracy of both models. MSE and AARD values were evaluated from Eqs.10 & 11, respectively; while the coefficient of determination (R^2) values was estimated from Fig. 11. From the values of R^2, MSE and AARD shown in **Table 6**, the ANN predictions produced a higher regression coefficient and a negligible deviation from experimental values when compared to the RSM predictions. This confirms that ANN technique as against RSM technique portrayed better accuracy in capturing the non-linear nature of the coagulation process.

$$MSE = \frac{1}{n}\sum_{i=1}^{n}\left(y_{i,}\,predic. - y_{i,}\,\exp.\right)^2 \tag{10}$$

$$AARD(\%) = \frac{1}{n}\sum_{i=1}^{n}\left(\left|\frac{\left(y_{i,}\,predic. - y_{i,}\,\exp.\right)}{\left(y_{i,}\,\exp.\right)}\right|\right)\times 100 \tag{11}$$

Where; $y_{i,predic.}$, $y_{i,\exp.}$ and n are final turbidity obtained by the predicted model, the experimental data and the number of experimental data, respectively.

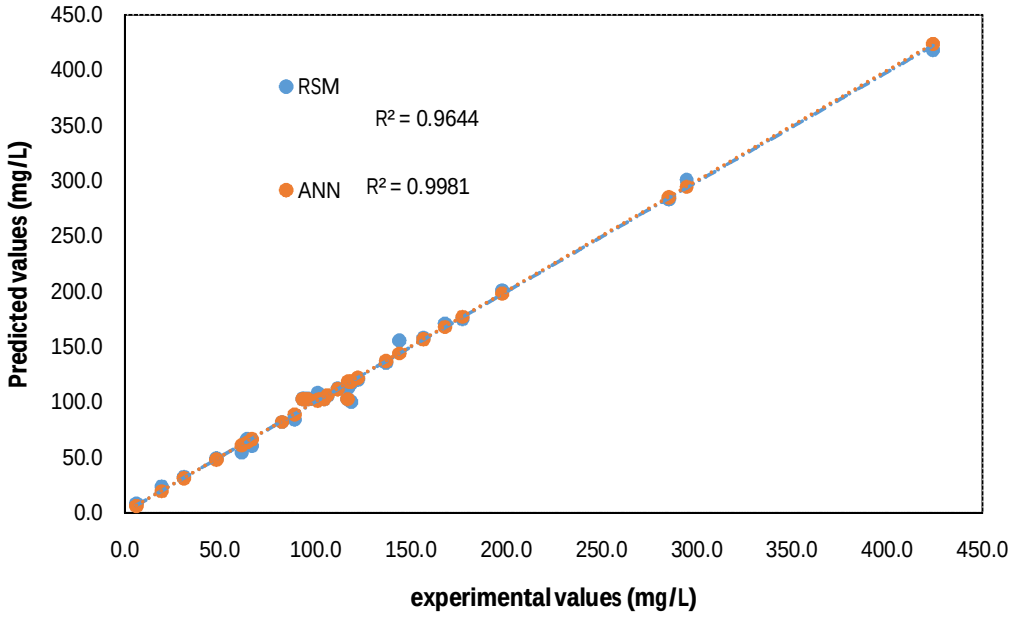

Fig. 12: RSM and ANN model appraisal

Table 6: Comparison of predictive competency of RSM and ANN

	RSM	ANN
MSE	37.78	13.11
R^2	0.9641	0.9981
AARD	5.93	1.43

Fig. 13 shows the comparative parity plot for the RSM, ANN models and the experimental data versus experimental run number. High correlation could be observed between the ANN and experimental data points. Meanwhile, in comparison with the experimental data point, the RSM data point showed significant deviations especially at run numbers 14, 22 and 23; with magnitudes of 5.6, 11.4 and 18.4, respectively. The correlation depicted by ANN data points in relation to the experimental values further gave credence to the superiority of ANN model over the RSM model with respect to the present study.

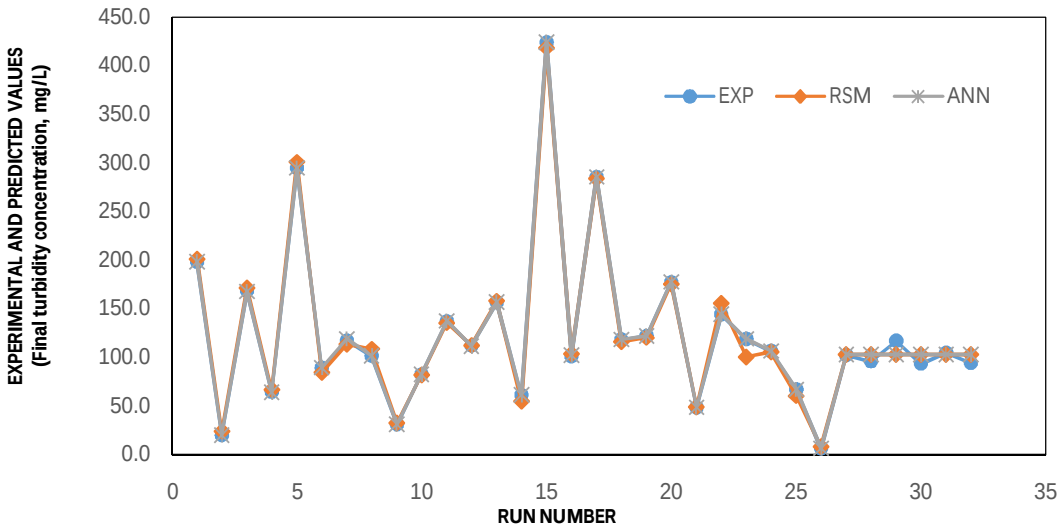

Fig. 13: A plot depicting the comparison between the experimental and predicted values for the ANN and RSM models

3.8. Optimization using ANN-Genetic Algorithm (ANN-GA) technique

The objective of process optimization is to search for the optimum process conditions to establish the minimum final turbidity. In this approach, the ANN-GA was used to generate the model values. Eqs. 12 – 16 show the selected range of constraints for each variable. Also, the technique of hybrid ANN-GA algorithm used in this work is illustrated in Fig. 14.

$$6.5 \leq pH \leq 7.5 \tag{12}$$

$$1.0\,g/L \leq dosage \leq 1.5\,g/L \tag{13}$$

$$183\ mg/L \leq initialcon\ c. \leq 250\ mg/L \tag{14}$$

$$310\ K \leq Temp.\ \leq 345\ K \tag{15}$$

$$30\ \text{min}. \leq settling\ time \leq 50\ \text{min}. \tag{16}$$

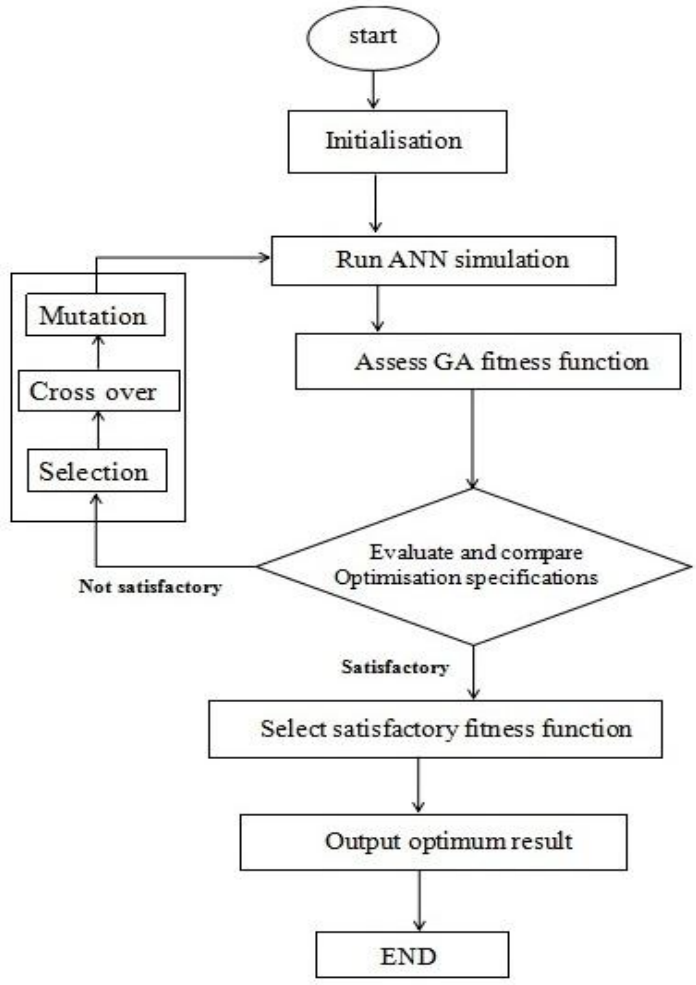

Fig. 14: Flow chart of combining ANN-GA optimisation technique.

However, based on afore mention evaluation an optimal final turbidity of 4.96 mg/L was obtained pH = 6.7, dosage = 1.003 g/L, initial conc. = 182.2 mg/L, coagulation temperature = 345 K and settling time = 36 min. Duplicate validation experiments were conducted in order to uphold the optimal predicted value. Using the optimum variable conditions, the average final turbidity obtained was 5.53 ± 0.24 (mg/L). The treated effluent obtained after the validation experiment was characterized and the results are shown on Table 7. The characterization result shows that the model prediction was in agreement with the experimental value.

Table 7: Post optimal characterization results of the abattoir waste water

Parameter	Treated abattoir
Final turbidity concentration (mg/L)	5.3
Total suspended solids (mg/L)	2.5
Total solids (mg/L)	3.1
Biological oxygen demand (mg/L)	8.6
Chemical oxygen demand (mg/L)	152
pH	8.1
Odour	Slightly alkaline
Colour	Clear colourless

4. **Conclusion**

In this work, the coag-flocculation of abattoir waste water was studied using HPA derived from raw CB. RSM and ANN modelling techniques were comparatively used in predicting the final turbidity of the effluent. Statistical techniques (R^2 and RMSE) were employed in selecting the most appropriate hidden number of neurons. Multi-layer neural network (5-7-1) was chosen to develop accurate and complex nonlinear relationship. From the results of the comparative analysis, ANN model was found to perform better in capturing the non-linear nature of the system. Process optimization using ANN-GA technique gave an optimum value of 4.92 mg/L for final effluent turbidity at pH = 6.7, dosage = 1.003 g/L, initial conc. = 182.2 mg/L, coagulation temperature = 345K and settling time = 36 min. This value was validated by a set of duplicate experiments producing an average value of 5.53 ± 0.24 (mg/L) which is in close agreement with the predicted value.

References

Mshelbwala GM, (2013). National Livestock Policy Focal Point Presentation – Nigeria. Paper presented at Side-meeting of NLPFPS on VET-GOV programme engagement / targetting and capacity building facilitation Abidjan, Cote D'ivoire.

Ogbeide, O. A., 2015. Meat Industry Development in Nigeria: Implications of the Consumers' Perspective. Mayfair Journal of Agribusiness Management. 1, 59 - 75.

Ohale, P.E., Onu,C. E., Nwabanne, J. T., Aniagor, C. O., Okey-Onyesolu, C. F., Ohale, N. J., 2022. A comparative optimization and modeling of ammonia–nitrogen adsorption from abattoir wastewater using a novel iron-functionalized crab shell. Applied Water Science 12:193: 1 – 27. https://doi.org/10.1007/s13201-022-01713-4

Obi, C. C., Nwabanne, J. T., Igwegbe, C. A., Ohale, P. E., Okpala, C. O. (2022). Multi-characteristic optimization and modeling analysis of electrocoagulation treatment of abattoir wastewater using iron electrode pairs. Journal of Water Process Engineering, 49, 103136. https://doi.org/10.1016/j.jwpe.2022.103136

Kundu, P., Debsarkar, A., Mukherjee, S., 2013. Treatment of Slaughter House Wastewater in a Sequencing Batch Reactor: Performance Evaluation and Biodegradation Kinetics. Hindawi Publishing Corporation BioMed Research International. 11, 1 - 15. https://doi.org/10.1155/2013/134872

Bazrafshan, E., Zakeri, H.R., Vieira, M.G.A., Derakhshan, Z., Mohammadi, L., Mohammadpour, A., Mousavi Khaneghah, A., (2022). Slaughterhouse Wastewater Treatment by Integrated Chemical Coagulation and Electro-Fenton Processes, Sustainability 14, 11407. https://doi.org/10.3390/su141811407

Menkiti, M. C., Sekaran, G., Ugonabo, V. I., Menkiti, U. N., Onukwuli, O. D., (2015). Factorial Optimisation and Kinetic studies of coagulation-flocculation of brewery effluent by crab shell coagulant. Journal of Chinese Advanced Materials Society.4, 36 – 61. https://doi.org/10.1080/22243682.2015.1048287

Ohale, P. E., Onu, C. E., Ohale, N. J., Oba, S. N., (2020). Adsorptive kinetics, isotherm and thermodynamic analysis of fishpond effluent coagulation using chitin derived coagulant from waste Brachyura shell, Chemical Engineering Journal Advances, 4, 100036. https://doi.org/10.1016/j.ceja.2020.100036

Menkiti, M. C., Ejimofor, M., (2016). Experimental and artificial neural network application on the optimization of paint effluent (PE) coagulation using novel acatinodea shell extract (ASE). JWPE. 10, 172-187. https://doi.org/10.1016/j.jwpe.2015.09.010

Al-Mutairi, N. Z., Hamoda, M. F., Al-Ghusain, I., (2004). Coagulant selection and sludge conditioning in a slaughterhouse wastewater treatment plant. Bioresource Technology. 95, 115 – 119. https://doi.org/10.1016/j.biortech.2004.02.017

Amuda, O. S., Alade, A., (2006). Coagulation/flocculation process in the treatment of abattoir wastewater. Desalination 196, 22–31. https://doi.org/10.1016/j.desal.2005.10.039

Aquilar, M. I., Sáez, J., Llorens, S. M., Ortuño, J. F., Meseguer, V., Fuentes, A., (2005). Improvement of coagulation-flocculation process using anionic polyacrylamide as coagulant aid. Chemosphere.58,47 – 56. https://doi.org/10.1016/j.chemosphere.2004.09.008

Mahtaba, A., Tariq, M., Shafiq, T., Nasir, A., (2009). Coagulation/adsorption combined treatment of slaughterhouse wastewater. Desalination and Water Treatment 12, 270–275. https://doi.org/10.5004/dwt.2009.952

Katayon, S., Megat-Mohd, M. J., Asma, M., Abdul-Ghani, L. A., Thamer, A. M., Azni, I., Ahmad, J., Khor, B. C., Suleyman, A. M., (2006). Effects of storage conditions of Moringa Oleifera seeds on its performance in coagulation. Bioresource Technology 97, 1455–60. https://doi.org/10.1016/j.biortech.2005.07.031

Ghedjemis, A., Riad Ayeche, R., Maya Kebaili, M., Ali Benouadah, A., Laurent Frédéric Gil, L. (2022). Application of natural hydroxyapatite in the treatment of polluted water: Utilization of dromedary bone as bioadsorbent, International of applied ceramic technology. https://doi.org/10.1111/ijac.14041

Choumane, F. Z., Benguella, B., Maachou, B., Saadi, N. (2017). Valorisation of a bioflocculant and hydroxyapatites as coagulation-flocculation adjuvants in wastewater treatment of the steppe in the wilaya of Saida (Algeria), Ecological Engineering 107, 152–159. http://dx.doi.org/10.1016/j.ecoleng.2017.07.013

Brazdis, R.I., Fierascu, I., Avramescu, S.M., Fierascu, R.C. (2021). Recent Progress in the Application of Hydroxyapatite for the Adsorption of Heavy Metals from Water Matrices. Materials, 14, 6898. https://doi.org/10.3390/ma14226898

Marrane, S. E., Dänoun, K., Allouss, D., Sair, S., Channab, B., Rhihil, A., Zahouily, M. (2022). A Novel Approach to Prepare Cellulose□g□Hydroxyapatite Originated from Natural Sources as an Efficient Adsorbent for Heavy Metals: Batch Adsorption Optimization via Response Surface Methodology. ACS Omega, 7, 28076−28092. https://doi.org/10.1021/acsomega.2c02108

Onu, C. E., Igbokwe, P. K., Nwabanne, J. T., & Ohale, P. E. (2022a). ANFIS, ANN, and RSM modeling of moisture content reduction of cocoyam slices. Journal of Food Processing and Preservation 46, 10 https://doi.org/10.1111/jfpp.16032

Ohale, P. E., Uzoh, C. F., Onukwuli, O. D. (2017). Optimal factor evaluation for the dissolution of alumina from Azaraegbelu clay in acid solution using RSM and ANN comparative analysis, South African Journal of Chemical Engineering 24, 43 – 54. https://doi.org/10.1016/j.sajce.2017.06.003

Nwadike, E. C., Abonyi, M. N., Nwabanne, J. T., Ohale, P. E. (2020). Optimization of Solar Drying of Blanched and Unblanched Aerial Yam using Response Surface Methodology, International Journal of Trend in Scientific Research and Development, 4 (3), 659 – 666.

Onu et al., (2022b). Modeling, optimization, and adsorptive studies of bromocresol green dye removal using acid functionalized corn cob, Cleaner Chemical Engineering 4, 100067. https://doi.org/10.1016/j.clce.2022.100067

Onu, C. E., Nwabanne, J. T., Ohale, P. E., Asadu. C. O. (2021). Comparative analysis of RSM, ANN and ANFIS and the mechanistic modeling in eriochrome black-T dye adsorption using modified clay, South African Journal of Chemical Engineering 36, 24 – 42. https://doi.org/10.1016/j.sajce.2020.12.003

Onu, C. E., Igbokwe, K. P., Nwabanne, J. T., Charles, O. C., Ohale, P. E. (2020). Evaluation of optimization techniques in predicting optimum moisture content reduction in drying potato slices, Artificial Intelligence in Agriculture 4, 39 – 47. https://doi.org/10.1016/j.aiia.2020.04.001

Emembolu, L. N., Ohale, P. E., Onu, C. E., Ohale, N. J. (2022). Comparison of RSM and ANFIS modeling techniques in corrosion inhibition studies of Aspilia Africana leaf extract on mild steel and aluminium metal in acidic medium, Applied Surface Science Advances, 11, 100316. https://doi.org/10.1016/j.apsadv.2022.100316

Jamil, S., Zhonghua, S., Mingshan, J., Zumin, G., Waqas, A. (2018). ANN and RSM based modeling for optimization of cell dry mass of Bacillus sp. strain B67 and its antifungal activity against botrytis cinerea, Biotechnol. Biotechnol. Equip., 32 (1), pp. 58-68. https://doi.org/10.1080/13102818.2017.1379359

Pakravan, P., Akhbari, A., Moradi, H., Azandaryani, A. H., Mansouri, A. M., Safari, M., 2015. Process modeling and evaluation of petroleum refinery wastewater treatment through response surface methodology and artificial neural network in a photocatalytic reactor using poly ethyleneimine (PEI)/titania (TiO2) multilayerfilm on quartz tube. Appl Petrochem Res. 5, 47–59. https://doi.org/10.1007/s13203-014-0077-7

Sodeifian, G., Sajadian, S. A., Ardestani, N. S., 2016. Evaluation of the response surface and hybrid artificial neural network genetic algorithm methodologies to determine extraction yield of Ferulago angulata through super critical fluid. Journal of the Taiwan Institute of Chemical Engineers. 60, 165–173. https://doi.org/10.1016/j.jtice.2015.11.003

Brzezińska-Miecznikn, J., Haberko, K., Sitarz, M., Bućko, M. M., Macherzyńska, B. (2015). Hydroxyapatite from animal bones – Extraction and properties, Ceramics international, http://dx.doi.org/10.1016/j.ceramint.2014.12.041

Clesceri, L. S., Greenberg, A. E., and Eaton,A. D. Standard Methods for the Examination of Water and Wastewater, American Public Health Association, America Water Works Association, Water Environment Federation, Washington, DC, USA, 29th edition, 1998.

Coutts, R. T., 2008. In: Chatten,L. G., (ed). Pharmaceutical Chemistry – Instrumental Techniques. CBS Publishers and Distributors PVT Ltd., New Delhi, India, pp. 59 – 125.

Ohale, P. E., Nwajiobi, O. J., Onu, C. E., Madiebo, E. M., Ohale, N. J. (2022b). Solvent extraction of oil from three cultivars of Nigerian mango seed kernel: Process modeling, GA -

optimization, nonlinear kinetics and comparative characterization, Applied Food Research 2 (2), 100227. https://doi.org/10.1016/j.afres.2022.100227